Dual Port Antenna Combining Sensing and Communication Tasks for Cognitive Radio

Hamza Nachouane, Abdellah Najid, Abdelwahed Tribak, and Fatima Riouch

Abstract—**Dynamic spectrum access has been proposed as the effective solution to overcome the spectrum scarcity issue, supported by cognitive radio technology. Sensing and communication functions are both the most important tasks in cognitive radio systems. In this paper, an antenna system combining sensing and communication tasks is proposed to be integrated into cognitive radio front-ends. The sensing task is performed by means of an ultra-wideband quasi-omnidirectional antenna. Whilst the communication task is ensured by using a narrowband antenna. Both antennas have been designed on the same layer of an FR4 substrate, for manufacturing cost constraint. Therefore, the isolation between them must take into consideration. The measured mutual coupling of less than -18 dB is achieved over the whole impedance bandwidth. The proposed sensing antenna covers a wide range frequency bands ranging from 2 to 5.5 GHz. While the communication antenna operates at 2.8 GHz, and by adding inductors to the antenna, the resonant frequency can be tuned from 2.6 to 2.7 GHz. The whole antenna system was designed, fabricated, and tested. Measurement and simulation results prove the feasibility of the proposed structure for cognitive radio applications.**

Keywords—**Cognitive radio, microstrip antenna, UWB, coplanar waveguide, sensing and communication tasks, sensing antenna.**

I. Introduction

NOWADAYS, the exponential growth in terms of wireless users and bandwidth-hungry applications and services, such as video conferencing and streaming, introduces a significant issue for wireless communication systems. Given that all radio-frequency (RF) resources are already allocated by the Federal Communications Commission (FCC). Nevertheless, according to recent measurements done by the FCC [1], the usage of spectrum is inefficient which provides a lot of spectrum holes, known as white spaces. These measures show, in fact, that a very important parts of spectrum remain underutilized or unused for 90% of the time [2], as shown in Fig. 1. To overcome this issue, the dynamic spectrum access (DSA) technique has been proposed [3]. The DSA technique can be considered as a wise solution to overcome the spectrum scarcity. It consists of exploiting the existing RF spectrum in an opportunistic manner, in order to detect the white spaces and then use them, so that the spectrum resources will be exploited in a more efficient way [4]. To bring this solution to reality, many solutions have been put forth. One of the proposed solutions is the cognitive radio (CR) paradigm [5], [6]. CR is an intelligent system which is able of continuously supervise the spectrum (sensing task),

H. Nachouane , A. Najid, A. Tribak, and F. Riouch are with Departement of Electronics, Microwaves and Optics, National Institute of Posts and Telecommunications, Rabat, Morocco, (e-mail: nachouane@inpt.ac.ma; najid@inpt.ac.ma; tribak@inpt.ac.ma; riouch@inpt.ac.ma).

in order to detect the white spaces. When the CR system detects the available frequency bands, it tunes dynamically its parameters to communicate within these unused frequency bands (communication task).
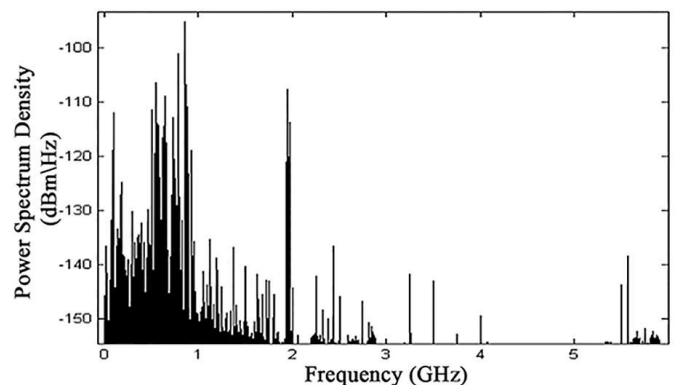

Fig. 1. Measurement of 0-6 GHz spectrum utilization [7].

Thus, the RF front-end of such system must ensure its main functionalities, which are the sensing and communication tasks. To ensure the sensing task, the antenna must operate over a wide range of frequency bands, with the intention of covering almost all spectrum bands as possible. Although to ensure the communication task, the system must behave as a narrowband antenna, to focus its power on the signal-of-interest while tuning out any interferences. According to the literature, antennas used in CR systems can be divided into two categories [8], the one- and the two-port structures. The first category consists of using one antenna that can act as a UWB or narrowband, depending on the requested task [9]–[11]. While the second category consists of using an antenna system composed of two antennas [12]–[14], one for sensing and the other for communication task. The two-port structure category exhibits good performance, in terms of its ability to provide both sensing and communication tasks simultaneously. Contrariwise the one-port structure, the two tasks cannot be performed at the same time. Nevertheless, the two-port structure provides one drawback which is the mutual coupling between the two elements. Therefore, the proposed structure must be properly designed in order to get more isolation between both antennas.

Several papers presenting the integration of narrowband/UWB antennas have been recently reported in the literature. In [15], a UWB disk monopole antenna and narrowband antenna designed on each side of the substrate have been presented. To enhance the isolation between them, a microstrip

TABLE I

COMPARISON OF PROPOSED ANTENNA SYSTEM WITH OTHER REPORTED ANTENNA SYSTEM FOR CR APPLICATIONS

Published literature	Sensing bandwidth (GHz)	Communication frequency (GHz)	Isolation (dB)	Size (mm^2)
[13]	$4 - 6$	5.125	10	32×54
[15]	$5.4 - 10,1$	9.3	17	40×31
[16]	$3.6 - 10 \ (-6dB)$	5.5	10	60×50
[17]	$3.1 - 11$	7.22 ; 4.125	10	65.5×58
[18]	$5.1 - 10.9$	5.76	30	42×28
[19]	$3.1 - 10.6$	8.8	10	27×21
[20]	$2.6 - 11$	5.25	15	58.7×77
Proposed system	$2 - 5.5$	2.8	18	80×65

open-loop resonator was used in order to introduce a band-stop at the undesired frequency bands. The narrowband antenna uses the disk monopole as a ground plane. As well for [16], the authors introduce a two-port antenna system that integrates two antennas, each one is designed on a side of the substrate. In order to get the narrowband response, two slots are used to act as a band-pass filter to suppress frequencies outside the desired frequency band. The narrowband antenna operates between 5 and 6 GHz. While the UWB antenna covers from 3.5 to 8 GHz. The one-side antenna design was presented in [17], the UWB and narrowband antennas were designed on the top side of the substrate. The UWB antenna covers the spectrum from 3.1 to 11 GHz, whilst the narrowband response was performed by two reconfigurable triangular-shaped elements; by rotating them, the narrowband antenna operates at 7.22 GHz (position 1), and 4.12 GHz (position 2). However, this design needs to be rotatable controlled by a field-programmable gate array (FPGA), which makes it very expensive. Table I summarizes the performance of the reported designs in terms of the sensing bandwidth, communication frequency, isolation, and their size. It can be clearly concluded that the majority of reported designs exhibit a mutual coupling less than -10 dB, and sensing higher frequencies. Therefore, it is impossible to integrate these antennas with modern wireless communications standards operate over lower frequency bands, such as 802.11n, 802.11ac, 3GPP LTE, 4G LTE-Advanced.

In this paper, an antenna system which can be suitable for RF front-end for cognitive radio systems is designed, simulated, fabricated, and measured. The antenna structure was designed on an FR4 substrate, with an overall size of $80 \times 65 \times 1.58 mm^3$. The antenna structure consists of two antennas fed by two coplanar waveguide (CPW) lines, and designed on each side of the substrate, as shown in Fig. 2, in order to get more isolation between them. The sensing task was performed by the UWB antenna which covers a wide range of frequency bands from 2 to 5.5 GHz. While the communication task was ensured by means of a narrowband antenna which can operate from 2.6 to 3 GHz. A good isolation has been achieved between the two antennas, which is better than 18 dB within the whole operating bandwidth. A prototype of the proposed antenna structure was fabricated and tested. The comparison between the simulated and measured results

shows good agreement, which proves the feasibility of the structure to be integrated into the RF front-end CR systems.

II. ANTENNA SYSTEM GEOMETRY

The configuration of the proposed antenna system is shown in Fig. 2. The two antennas and their ground plane were designed on the top side of a 1.58-mm-thick FR4 substrate with dielectric constant $\varepsilon_r = 4.3$ and loss tangent $\varphi = 0.02$. The total space occupied by the entire system is $80 \times 65 \times 1.58 mm^3$. The reason behind the choice of FR4 substrate is its low-cost, low-loss and its availability in the market. As mentioned above, the sensing and communication tasks, were performed by means of UWB and narrowband antennas, respectively, and were fed by two CPW lines, as shown hereafter. The CPW technology has been chosen, among other technologies such Substrate Integrated Waveguide (SIW), owing, in fact, to two reasons. Firstly, to create the ground plane on the top side of substrate as an obstacle between both antennas, in order to get the less mutual coupling as possible. Secondly, and most importantly, we consider that as future work the proposed design will incorporate active and passive components, such as diodes and capacitors, to make the antenna frequency and pattern reconfigurable; the CPW technology makes the integration of electronic components very easier than the microstrip or SIW technologies, since it prevents the costly and inductive via holes [21]. The designed UWB and narrowband
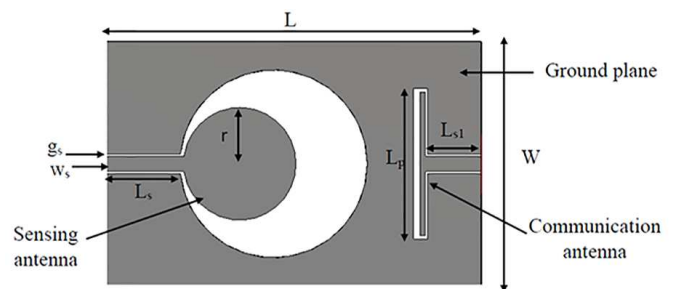

Fig. 2. Structure of the proposed antenna system.

antennas and their ground plane are combined together so as to achieve the final topology as shown in Fig. 2. The dimensions of each component are depicted in Table II.

As aforementioned, both antennas were fed by CPW lines. In order to get 50Ω input impedance, the dimensions of the

TABLE II
ANTENNA SYSTEM DIMENSIONS (IN MM)

L	W	W_s	g_s	r	L_s1	L_s2	L_p
80	65	4	0.5	15	14	20	40

feed line, as well as the two gaps, were calculated using equations mentioned in [21]:

$$Z_{in} = \frac{30\pi}{\sqrt{\varepsilon_{eff,t}}} \times \frac{K(K_t^{'})}{K(K_t)} \qquad (1)$$

$$\varepsilon_{eff,t} = \varepsilon_{eff} - \frac{\varepsilon_{eff} - 1}{\frac{g}{0.7 \times t} \times \frac{K(K)}{K^{'}(K)} + 1} \qquad (2)$$

$$\varepsilon_{eff} = 1 + \frac{\varepsilon_r - 1}{2} \times \frac{K(K^{'}) \times K(K_1)}{K(K) \times K(K_1^{'})} \qquad (3)$$

with,

$$K_t = \frac{w_t}{s_t}; K = \frac{w}{s}; s = w + 2 \times g \qquad (4)$$

$$K_1 = \frac{sinh(\frac{\pi w_t}{4h})}{sinh(\frac{\pi s_t}{4h})} \qquad (5)$$

with,

$$K_t^{'} = \sqrt{1 - K_t^2}; K^{'} = \sqrt{1 - K^2}; K_1^{'} = \sqrt{1 - K_1^2} \qquad (6)$$

where w, g, h, ε_r, and t are the feed line width, the gap, the substrate height, the permittivity, and the metal thickness, respectively. $K(K)$ and $K^{'}(K)$ represent the complete elliptic integral of the first kind and its complement.

Since the conductor is very thin, its thickness cannot be totally neglected. The non-zero thickness of the conductor leads us to:

$$w_t = w + \frac{1.25 \times t}{\pi} \times [1 + \ln(\frac{4\pi w}{t})] \qquad (7)$$

$$s_t = s - \frac{1.25 \times t}{\pi} \times [1 + \ln(\frac{4\pi w}{t})] \qquad (8)$$

By using these equations and those mentioned in [22], the dimensions of the narrowband antenna were carefully calculated, in order to operate at the desired frequency. The gaps between the antenna and the ground plane were optimized by means of the electromagnetic (EM) simulation software CST Studio Suite. The real and imaginary parts of the input impedance were presented in Fig. 3. It can be clearly observed that the real part presents different values of 50Ω at different frequencies. Since the imaginary part of the impedance represents the power that is stored in the antenna near-field, which is non-radiated power, so it must be canceled. The only frequency that provides this requirement (50Ω impedance with zero reactance) is 2.8 GHz, which verifies the good matching around this frequency, as we will conclude shortly from measurements.
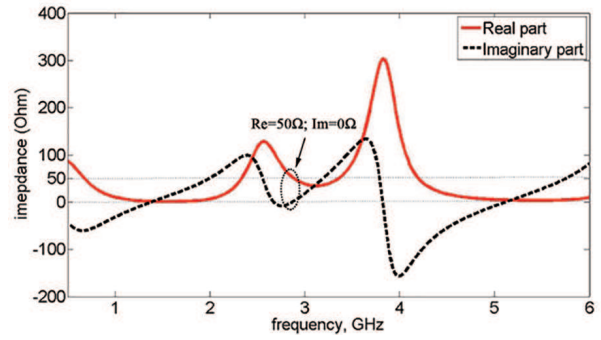

Fig. 3. Real and imaginary parts of the narrowband antenna impedance.

For the UWB sensing antenna, the width and the gaps dimensions were also calculated using equations mentioned before. While the radius of the circular disc was calculated by means of the equations mentioned hereafter [22]:

$$r = \frac{F}{\sqrt{1 + \frac{200h}{\pi \varepsilon_r F} \left[\ln \left(\frac{F\beta}{200h} \right) + 1.7726 \right]}} \qquad (9)$$
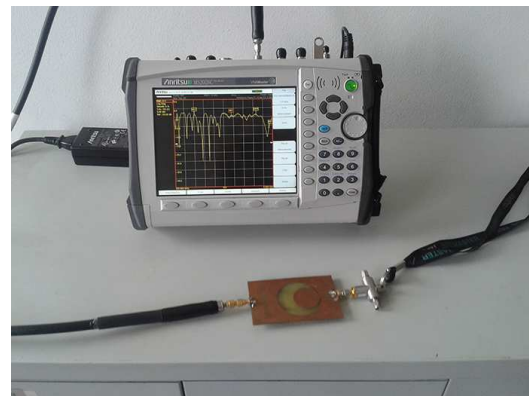
with,

$$F = \frac{8.791 \times 10^9}{f_r \sqrt{\varepsilon_r}} \qquad (10)$$

where r is the radius of circular patch and f_r is the resonant frequency.
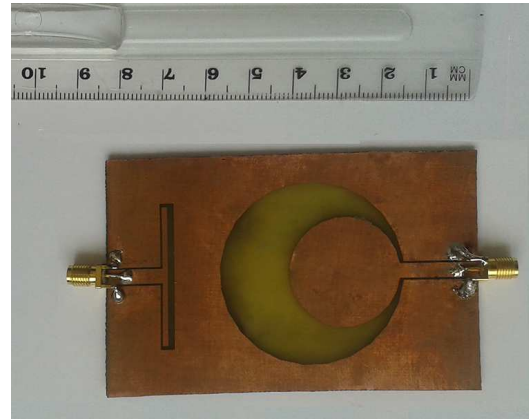
(a)

(b)

Fig. 4. Fabricated proposed antenna system (a) and its measurement equipment (b).

III. MEASURED AND SIMULATED RESULTS

The antenna system was designed and simulated using CST Studio Suite and ANSYS HFSS, which are based on different numerical methods. A prototype of the structure was fabricated and tested for scattering parameters using an Anritsu Vector Network Analyzer model #MS2028C at Antenna and Microwave Lab at INPT. A photograph of the fabricated prototype and its measurement setup are depicted in Fig. 4.

The proposed UWB sensing antenna covers a wide frequency band ranging from 2 to 5.5 GHz, which is 93.33% around the center frequency 3.75 GHz, and yields an impedance bandwidth ratio of 2.75:1. The simulated and measured reflection coefficient for sensing antenna are compared in Fig. 5. The measurement results are in close agreement with the simulated ones. The discrepancy between the three curves may be explained by the inevitable proximity of SMA connector to the slot of the CPW and also might be due to the tolerances in manufacturing and hand-cut errors. In addition, the different boundary conditions of both EM simulation software may highly influence the reflection coefficients as well as the radiation patterns. According to Fig. 5, it is clear that around 1.5 GHz, a resonant frequency appeared, and this may be caused by the spurious reflections from cable and the SMA connector that are not incorporated in the EM simulation.
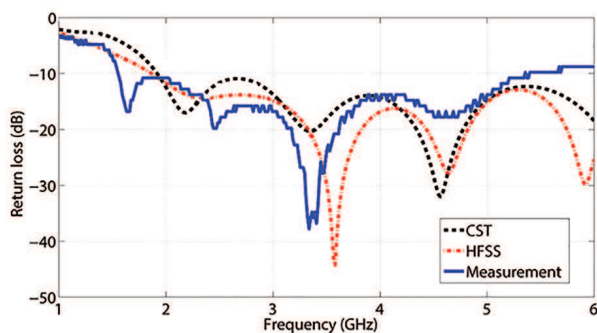

Fig. 5. Simulated and measured reflection coefficient for the UWB sensing antenna.
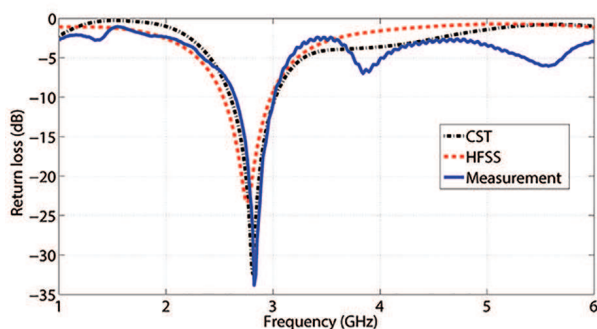

Fig. 6. Simulated and measured reflection coefficient for the narrowband antenna.

The narrowband communication antenna operates at 2.8 GHz. As shown in Fig. 6, the measured and simulated reflection coefficient show that we obtain a narrow bandwidth and

good matching around the desired frequency, 2.8 GHz, which are about 400 MHz and -35 dB, respectively. The measured and simulated results show, in fact, a very good agreement verifying the proposed structure. However, a small discrepancy was observed at higher frequencies, which is due to parasitic capacitance created across the gap sides. In order to make the communication antenna operates at different frequency bands, two inductors with different values can symmetrically be loaded to the patch antenna edge, as shown in Fig. 7. As observed from reflection coefficient curves in Fig. 8, the resonant frequency of communication antenna can be tuned from 2.6 to 2.7 GHz, when the loading inductors are chosen as 2×5.6 and 2×10 nH, respectively. Conventional surface-mounted chip inductors used must have 1-mm-length of package size to fit the gap width, the commercial inductors of 5.6 and 10 nH are LL1005-FHL5N6S and LL1005-FHL10NJ, respectively. The inductors are intended to extend the electrical length of communication antenna, in order to operate at lower frequency bands. For future work, the inductors can be replaced by diodes to get more flexibility.
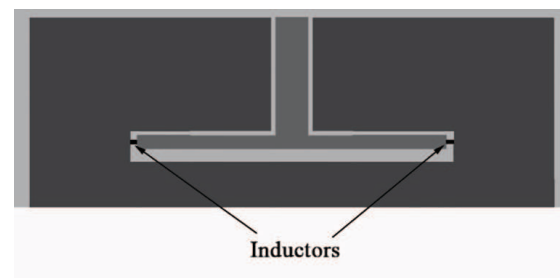

Fig. 7. Schematic diagram of the communication antenna with inductors loading.
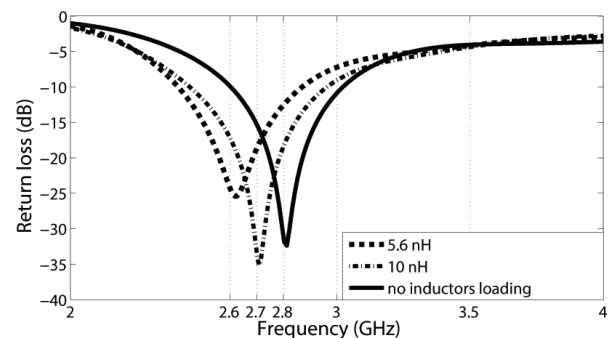

Fig. 8. Frequency-tuning characteristics of the communication antenna.

Since both antennas were designed on the same side of the substrate. Therefore, we must take it into account the isolation, which is a very required feature. In order to measure the coupling between the two antennas, the transmission coefficient is measured. Fig. 9 depicts the isolation between the UWB sensing and narrowband communication antennas. As we can see from the results, the measured isolation is better than 18 dB throughout the operational bandwidth. Compared to other reported designs shown in Table I, the proposed antenna system exhibits good performance in terms of isolation.
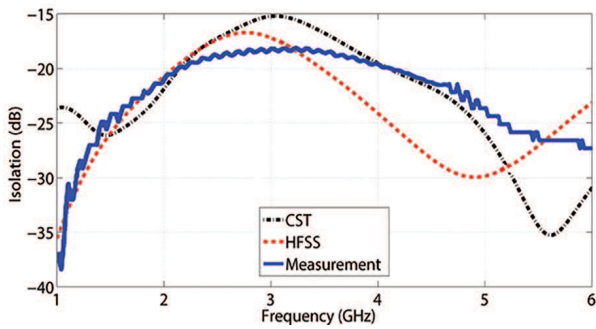
Fig. 9.   Simulated and measured isolation between antennas.

basic required feature of the sensing task is the omnidirectional radiation pattern; in order to scan the environment in terms of space (geographic location) and RF spectrum by covering different angles. The computed 2-D gain patterns of the UWB sensing antenna in the yz-cut (E-plane) and xz-cut (H-plane) planes at different frequencies are presented in Fig. 12. At all these frequencies, the sensing antenna presents a quasi-omnidirectional feature. The peak gain at 2.5, 3.5, 4.5, and 5.5 GHz are 3.92, 4.46, 5.78, and 7.7 dBi, respectively.

In order to further understand the isolation mechanism, the simulated surface current distributions of both antennas are investigated and shown in Fig. 10-11. It is evident that, when the sensing antenna is fed, as shown in Fig. 10, high current density can be observed at the feed line as well as the edge of the ground circular slot, which contributes for radiation. Meanwhile, the current excited at the port of communication antenna is almost nil, which proves that both antennas are totally decoupled. Whereas, when the communication antenna is fed, as shown in Fig. 11, the port of sensing antenna is completely isolated and the high current density is concentrated solely at the edge of the narrowband radiator. This demonstrates that the current coupling from sensing to communication antennas and vice versa is very low. This results in an efficient integration with low mutual coupling between the two ports.
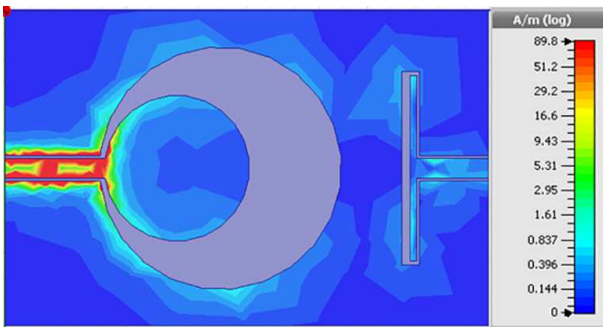

Fig. 10.   Surface current distributions for sensing antenna at 2.8 GHz.

(a)

(b)

Fig. 12.   Radiation patterns for UWB sensing antenna, (a) $\varphi = 0^o$ and (b) $\varphi = 90^o$.

The UWB sensing antenna exhibits the same characteristic as the printed circular monopole antennas, which is the quasi-omnidirectional radiation pattern. Nevertheless, in the yz plane ($\varphi = 90^o$) an asymmetric with respect to the x-axis is noteworthy. As we can see, the level of radiation is lower at $\theta = 270^o$ compared to $\theta = 90^o$, and this can be explained simply by the localization of the narrowband antenna in this direction, which slightly affects the sensing antenna behavior.
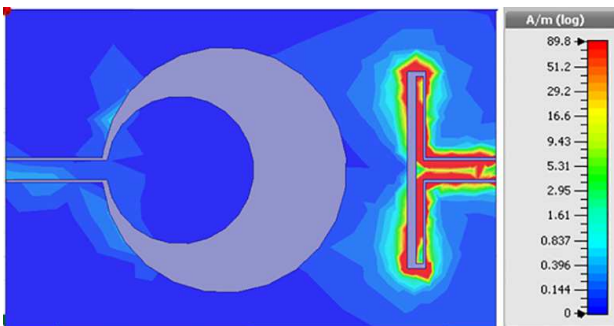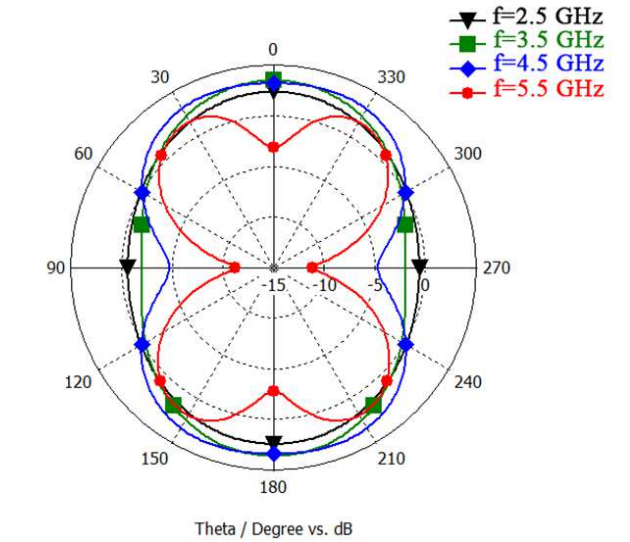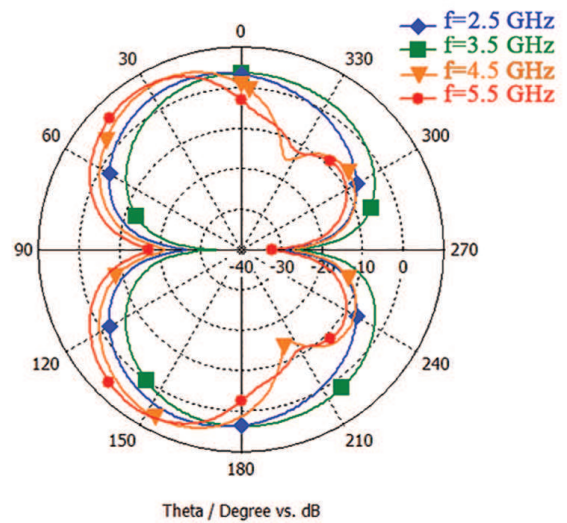

Fig. 11.   Surface current distributions for communication antenna at 2.8 GHz.

As aforementioned, the sensing task requires a wide bandwidth antenna to cover different frequency bands. But another

However, the radiation pattern shape at different frequencies do not drastically change, which concludes that the UWB sensing antenna satisfies the omnidirectional feature and have stable radiation patterns over the whole operating frequency band. In addition, the computed radiation patterns of the narrowband antenna at its resonant frequency in the xz- and yz-planes are shown in Fig. 13. These patterns were taken at the operating frequency, 2.8 GHz, and the peak gain is about 6.05 dBi. It is evident from the pattern that, the communication antenna is directional toward 0° and 180° because of the shape of antenna toward the corresponding directions. By placing two antennas in the same layer of the substrate, that might influence the current distributions on each and therefore causing some changes in the radiation patterns. Thus, some degradation of radiation is inevitable, seen that the CR system requires the employment of two antennas in close proximity.
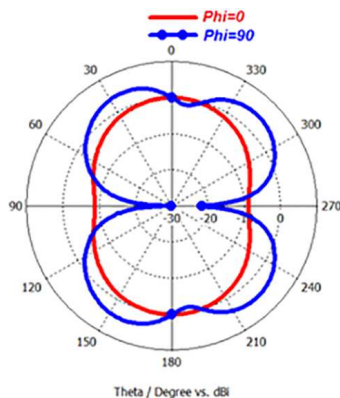

Fig. 13.   Radiation patterns for narrowband antenna at 2.8GHz, in xz cut ($\varphi = 0^o$) and yz cut ($\varphi = 90^o$).

When evaluating the performance of an antenna system that incorporates two antennas, the envelope correlation coefficient (ECC) is a critical parameter to take into account. It indicates how the radiation patterns of both antennas are uncorrelated. The antenna system diversity will be better if the ECC has lower values over the impedance bandwidth. The ECC ρ_e can be calculated using only the scattering parameters instead of radiation patterns, as it has been found in [23]:

$$\rho_e = \frac{|S_{11}^* S_{12} + S_{21}^* S_{22}|^2}{\left(1 - |S_{11}|^2 - |S_{21}|^2\right)\left(1 - |S_{22}|^2 - |S_{12}|^2\right)} \quad (11)$$

From Fig. 14, it can be concluded that the proposed antenna system exhibits a very low ECC values, between 0 and 0.2, over the operating bandwidth. This demonstrates that the radiation patterns of both antennas are perfectly uncorrelated, which means that there will be no overlap between sensing and communication antennas during the operation process.

Based on the three-antenna method [24], the peak gain of the proposed antenna system was measured at specific frequencies. This method is used instead of other methods because only one sample of the proposed antenna system is available. By using Friis transmission equation, the gain can be calculated at different frequencies. Table III presents the performance of proposed antenna system in terms of bandwidth, center frequency, and peak gain.
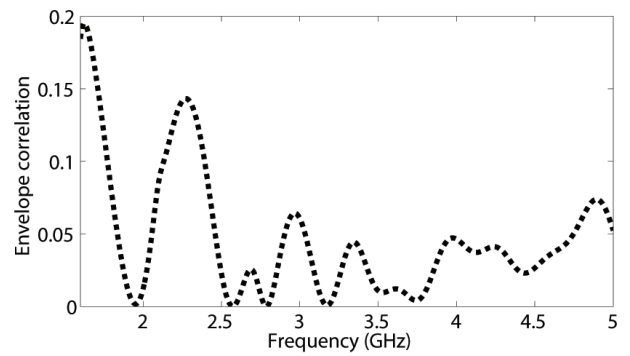

Fig. 14.   Calculated envelope correlation coefficient from S-parameters.

TABLE III
ANTENNA SYSTEM PERFORMANCES

	UWB sensing antenna	Communication antenna
Bandwidth (GHz)	3.5	0.4
Center frequency (GHz)	3.75	2.8
Peak gain (dBi)	5.81	6.6

The measured gain of the communication antenna is about 6.6 dBi, around its resonant frequency 2.8 GHz, while the measured gain of the sensing antenna is about 5.81 dBi around the center frequency 3.75 GHz.

IV. CONCLUSION

In this paper, a novel combined antenna system for cognitive radio front-ends is proposed, fabricated, and measured. It consists of two antennas, the first one is a quasi-omnidirectional UWB antenna for spectrum sensing, which covers the frequency bands from 2 to 5.5 GHz. While, the second one is a narrowband dipole antenna responsible for communication at the desired frequency, 2.8 GHz. However, it can be reconfigurable by loading different inductors into the antenna, the resonant frequency can be tuned from 2.6 to 2.7 GHz, as seen previously. Both antennas were properly designed on the same side of the cheap FR4 substrate, for space and manufacturing cost constraints. In order to prove the feasibility of the proposed structure, a prototype of the proposed antenna was fabricated and tested. A measured mutual coupling of less than -18 dB was achieved over the whole impedance bandwidth. The measured and simulated gain of the proposed antenna system are in good agreement. Furthermore, the radiation patterns of both antennas are perfectly uncorrelated, as the ECC indicated, which means that both antennas are totally decoupled. The good agreement between simulated and measured results are achieved, and since it covers the spectra of IEEE 802.11ac and 802.11n (2.5/5 GHz), UMTS2000 (2.1-2.2 GHz), and WiMax (2.3-2.5/3.4-3.5 GHz) systems, the proposed antenna system is a good candidate to be integrated into the RF front-ends for cognitive radio systems operating at these bands. Table III summarizes the performance of the fabricated proposed antenna system.

As future work, in order to achieve the frequency reconfigurability in such way to get the antenna operates at different

frequencies, passive and active components can be integrated into the narrowband antenna.

ACKNOWLEDGMENT

REFERENCES

[1] Federal Communications Commission, Spectrum Policy Task Force, "Report of the Spectrum Efficiency Working Group," November 2002.

[2] Federal Communications Commission, Facilitating Opportunities for Flexible, "Efficient and Reliable Spectrum Use Employing Cognitive Radio Technologies," notice of proposed rulemaking and order, FCC 03-322, December 2003.

[3] N. Kaabouch and W. C. Hu, *Handbook of Research on Software-Defined and Cognitive Radio Technologies for Dynamic*, University of North Dakota, US Spectrum Management, 2014.

[4] Q. Zhao and B. M. Sadler, "A survey of dynamic Spectrum Access," *IEEE Signal Processing Magazine*, pp. 79-89, May 2007.

[5] L. Berlemann and S. Mangold, *Cognitive Radio and Dynamic Spectrum Access*, John Wiley & Sons, Inc., 2009.

[6] J. Mitola and G. Q. Maguire, "Cognitive radios: Making Software Radios More Personal," *IEEE Personal Communications*, Vol. 6, No. 4, pp. 13-18, 1999.

[7] J. Yang, *Spatial Channel Characterization for Cognitive Radios*. MS Thesis, UC Berkeley, 2004

[8] M. Al-Husseini, K. Y. Kabalan, A. El-Hajj and C. G. Christodoulou, "Reconfigurable microstrip antennas for cognitive radio," in *Advancement in Microstrip Antennas with Recent Applications*, Prof. Ahmed Kishk (Ed.), chapter 14, InTech Publication, pp. 337-362, 2013.

[9] H. Nachouane, A. Najid, A. Tribak, and F. Riouch, "Reconfigurable Antenna Combining Sensing and Communication Tasks for Cognitive Radio Applications," in *Mediterranean Conference on Information and Communication Technologies*, Saidia, Morocco, May 7-9, 2015.

[10] P. Y. Qin, F. Wei, and Y. J. Guo, "A Wideband to Narrowband Tunable Antenna Using A Reconfigurable Filter," *IEEE Transactions on Antennas and Propagation*, vol. 63, no. 5, pp. 2282-2285, May 2015.

[11] M. R. Hamid, P. Gardner, P. S. Hall, and F. Ghanem, "Switched-Band Vivaldi Antenna," *IEEE Transactions on Antennas and Propagation*, vol. 59, no. 5, pp.1472-1480, 2011.

[12] R. Hussain, and M. S. Sharawi, "A Cognitive Radio Reconfigurable MIMO and Sensing Antenna System," *IEEE Antennas and Wireless Propagation Letters*, vol. 14, pp. 257-260, 2015.

[13] E. Ebrahimi, and P. S. Hall, "Integrated wide-narrowband antenna for multiband applications," *Microwave and Optical Technology Letters*, vol. 52, no. 2, pp. 425-430, February 2010.

[14] Y. Tawk, J. Costantine, and C. G. Christodoulou, "A rotatable reconfigurable antenna for cognitive radio applications," *IEEE Radio and Wireless Symposium (RWS)*, pp. 158-161, 16-19 January 2011.

[15] J. R. Kelly, P. S. Hall, P. Gardner, and F. Ghanem, "Integrated narrow/band-notched UWB," *Electronics Letters*, vol. 46, no. 12, pp. 814-816, 2010.

[16] F. Ghanem, P. S. Hall, and J. R. Kelly, "Two port frequency reconfigurable antenna for cognitive radios," *Electronics Letters*, vol. 45, no. 11, pp. 534-536, 2009.

[17] Y. Tawk, and C. G. Christodoulou, "A new reconfigurable antenna design for cognitive radio," *IEEE Antenna and Wireless Propagation Letters*, vol. 8, pp. 1378-1381, 2009.

[18] W. Lu, Z. Zhang, and H. Zhu, "Integrated Wideband and Narrowband Antenna with Low Mutual Coupling for Cognitive Radio Applications," in *International Conference on Microwave and Millimeter Wave Technology (ICMMT)*, vol.3, pp. 1-4, 5-8 May 2012.

[19] Y. Li, W. Li, and R. Mittra, "Integrated Dual-Purpose Narrow / Ultra-Wide Band Antenna for Cognitive Radio Applications," in *Antennas and Propagation Society International Symposium (APSURSI)*, pp. 1-2, 8-14 July 2012.

[20] G. Augustin, B. P. Chacko, and T. A. Denidni, "Dual Port Ultra Wideband Antennas for Cognitive Radio and Diversity Applications," in *Advancement in Microstrip Antennas with Recent Applications*, Prof. Ahmed Kishk (Ed.), InTech, 2013.

[21] R. N. Simon, *Coplanar Waveguide Circuits Components and Systems*, New York, John Wiley & Sons, pp. 11-83, 2001.

[22] C. A. Balanis, *Antenna Theory Analysis and Design*, 3rd edition, Hoboken, New Jersey, John Wiley & Sons, pp. 816-852, 2005.

[23] S. Blanch, J. Romeu, and I. Corbella, "Exact representation of antenna system diversity performance from input parameter description," *Electronics Letters*, vol. 39, no. 53, pp. 705-707, 2003.

[24] *IEEE Standard Test Procedures for Antennas,* ANSI/IEEE Std, 149-1979, Dec. 1979